PROCEEDINGS OF SCIENCE

A Monte Carlo Tool to Estimate Synchrotron X-ray Fluxes from EAS

Rodrigo Alberto Torres Saavedra[a,b,*] **and Roberto Aloisio**[a,b]

[a] *Gran Sasso Science Institute,*
Viale F. Crispi 7, L'Aquila (AQ), Italy
[b] *National Institute of Nuclear Physics – Gran Sasso National Laboratory,*
Via G. Acitelli 22, Assergi (AQ), Italy

E-mail: rodrigo.torressaavedra@gssi.it, roberto.aloisio@gssi.it

We present a new simulation framework to estimate X-ray synchrotron fluxes from extensive air showers at high altitude. Our simulation approach builds upon analytic expressions for the spectra of synchrotron radiation found in literature, which are combined with parameterized electron population distributions and longitudinal shower profile templates to calculate the expected synchrotron emission from the EAS. After accounting for photon propagation through the atmosphere, we then estimate the resulting photon fluxes at the detection plane. For a sub-orbital detector at 36 km, it was found that for near-horizontal showers $O(10^4)$ photon arrive to the detector position, distributed over an area ranging from $O(10\,\mathrm{m}^2)$ up to $O(100\,\mathrm{m}^2)$, depending on the photon energy band. These fluxes suggest that X-ray synchrotron emission is potentially a detectable signal for balloon-borne experiments.

39th International Cosmic Ray Conference (ICRC2025)
15–24 July 2025
Geneva, Switzerland

ICRC 2025
The Astroparticle Physics Conference
Geneva July 15-24, 2025

*Speaker

PoS(ICRC2025)417

1. Introduction

In recent years, the observation of extensive air showers (EAS) from sub-orbital and orbital altitudes has garnered increasing interest due to the advantages of these platforms with respect to direct or on-ground setups, namely: larger geometrical apertures and reduced atmospheric absorption. Examples of present, planned, and pathfinder mission that will adopt this observational approach include the Terzina payload onboard the NUSES satellite-mission [1], and balloon-borne experiments such as EUSO-SPB2 [2], PUEO [3], and PBR [4]. The development of these missions has driven significant efforts in modelling the fluorescence, Cherenkov, and radio emissions from EAS's as observed from sub-orbital and orbital altitudes.

An emission mechanism that, to the best of our knowledge, has not yet been modeled is X-ray synchrotron radiation from the charged secondaries (mostly e^+ and e^-, hereafter "electrons") in an EAS gyrating in the geomagnetic field. For relativistic electrons, this radiation is beamed, pulsed, and emitted in a band centered about the critical synchrotron frequency,

$$\omega_c = \frac{3}{2}\gamma^3 \omega_B \sin\alpha_p = \frac{3}{2}\gamma^2 \omega_L \sin\alpha_p = \frac{3}{2}\gamma^2 \left(\frac{q_e \|\vec{B}\|}{m_e c}\right) \sin\alpha_p \tag{1}$$

which is a function only of the magnetic field strength, $\|\vec{B}\|$, the electron's Lorentz factor, γ, and its pitch angle, α_p (the latter assumed to be 90 ° hereafter for simplicity). For a typical geomagnetic field strength of 0.5 G, electrons with energies of tens of MeV emit in the radio band, GeV in the optical, and high-energy (HE) electrons with $E \gtrsim 100$ GeV in the X-ray and γ-ray bands. Whereas radio synchrotron emission has been extensively modeled [5, 6], optical energy bands remain largely unexplored. In the optical band, Cherenkov radiation from the EAS is predominant, so there is little reward in modelling the synchrotron emission in this band. Contrastingly, the X-ray regime remains interesting because it probes the early stages of shower development, when electrons are on average more energetic.

To provide first-order predictions of the synchrotron X-ray fluxes as observed by a sub-orbital detector, we have developed a dedicated simulation tool. It convolves the single-particle synchrotron spectrum with parameterized electron energy distributions, evaluating this result along a template longitudinal profile, and propagating photons to a detection plane with distance- and energy-dependent atmospheric attenuation. For a detector at 36 km altitude, we find that near-horizontal showers (from 89 ° to 90 ° nadir angles) yield peak fluxes in the order of $O(10^4)$ transmitted photons distributed over a footprint area ranging from $O(10\,\mathrm{m}^2)$ up to $O(100\,\mathrm{m}^2)$, depending on the photon energy band. Section 2 of this work details the computational approach, whereas Section 3 discusses the obtained results.

2. The Computation Scheme

2.1 Emission from an Ensemble of Particles

In literature, the differential spectrum of the radiated energy by a single gyrating particle is proportional to the square of the Fourier transform of its radiation field [7]. This formalism can be extended to the case of a general ensemble by assigning a phase factor to each particle and summing

their contribution to the total field under the square modulus [8]. This approach introduces the possibility of coherent emission and is valid for the case of a distant observer, i.e. one such that the line-of-sight (LoS) vector is constant and the same for all particles. For X-ray synchrotron emission in the geomagnetic field, the phase coherence requirement is unrealistically stringent, $O(10^{-18})$ radians. Consequently, the emission can be safely regarded as non-coherent and the total emitted power as the sum of the single-particle contributions, with no particular constraints on the LoS vector. Further, if the computation is split into small grammage slices along the shower development the electron energies in each slice may be treated as approximately constant, and we may neglect the effect of backreaction on the spectrum [9]. Finally, as long as the HE electrons in the shower remain nearly aligned with the shower axis, their pitch-angle distribution can be approximated by the pitch-angle of the shower axis, $\alpha_{\mathrm{p,s}}$. Under these conditions, the number of photons emitted per unit grammage and photon energy reduces to the convolution of the single-particle synchrotron power spectrum with the electron energy distribution,

$$\frac{dN_\gamma}{dX dE_\gamma} = \frac{N_\mathrm{e}(X)}{\rho(X)c} \int dE_\mathrm{e} \frac{dn_\mathrm{e}}{dE_\mathrm{e}}(E_\mathrm{e}, X) \frac{1}{E_\gamma} \frac{dP}{dE_\gamma}^{(1)}(E_\mathrm{e}, E_\gamma, \alpha_{\mathrm{p,s}}, \|\vec{B}\|) \tag{2}$$

where E_e and E_γ are the electron and photon energies respectively, X the grammage along the shower axis, and $N_\mathrm{e}(X)$ and $\rho(X)$ the shower size and local atmospheric density at a given stage of shower development respectively. The details of this derivation will be explained in a paper under preparation by the same authors.

2.2 Electron Energy Distribution

As shown in Eq. 2, the number of photons emitted in an EAS strongly depends on the model chosen for the electron energy distribution. Therefore, in order to accurately model the expected synchrotron X-ray emissions, it is necessary to parameterize the electron energy distribution, and this parameterization must be valid simultaneously for: hadronic showers induced by UHE primaries, HE electrons, and young shower ages. Such parameterizations would rely on the concept of shower universality [10] or, namely, that the shape of the electron distributions for different showers is similar near the point of maximum shower development [11–14]. Arguably, this hypothesis starts to break down away from the shower maximum when the particle content of the shower decreases and shower-to-shower fluctuations become more relevant. Nevertheless, it is not the intention of this work to estimate synchrotron X-ray fluxes from a particular, individual shower, but rather to estimate the average flux that could be observed by a sub-orbital detector.

The Nerling [13] model was chosen for this work as it reportedly provides a better fit to simulations of hadronic showers with UHE primaries simulated with `CORSIKA` with respect to the models of Hillas [11] and Giller [12]. Given that we expect the maximum of X-ray synchrotron emission to occur at $s \sim 0.5$ for electrons with energies in the range 10^2 GeV to 10^3 GeV, and that the Nerling model has been explicitly validated down to $s = 0.8$ and up to $E_\mathrm{e} = 10$ GeV, we expect that we will extrapolate the Nerling model by 0.3 units in shower age (on average) and by two orders of magnitude in electron energy (at most). While we recognize the need for dedicated parameterizations of the energy distribution in this shower age and energy regime, we place such study beyond of the scope of this work and identify it simultaneously as the topic of a future study.

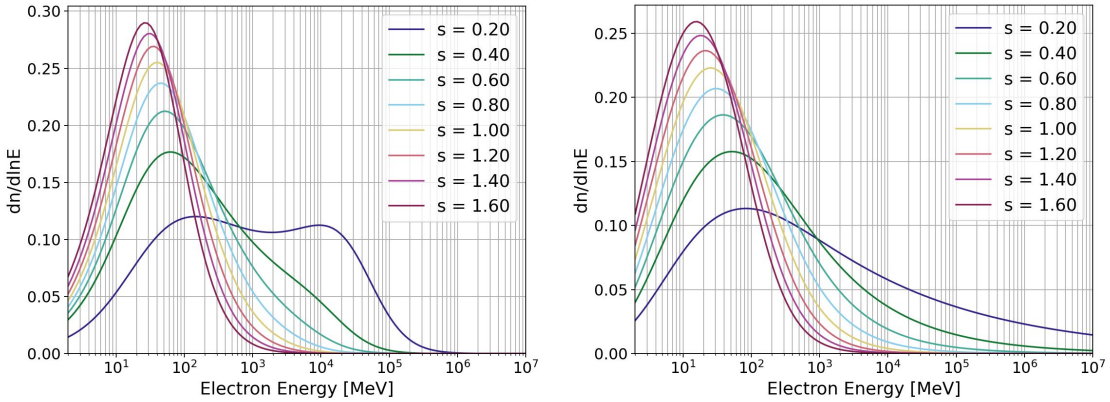

Figure 1: Electron energy distribution in an EAS according to Hillas (left) and Nerling (right) for different shower age values. The double-peak structure of the Hillas distribution (left) stems from its piece-wise definition, which models explicitly the two electron populations in young showers. The Nerling distribution has long tails that extend up to the HE regime, that may be understood as an effect of prompt HE electrons in the shower from hadronic interactions.

For the purposes of comparison, we also investigated X-ray synchrotron emissions using the Hillas model [11], which has been explicitly validated down to $s \sim 0.2$, albeit only for purely electromagnetic showers using dedicated MC simulations of photon-induced showers with energies up to 10^3 GeV. A side-by-side comparison of both models is shown in Fig. 1. With respect to the Nerling model, we find that the absolute number of emitted photons is significantly smaller, by about three orders of magnitude, and that the cumulative energy spectrum in the Hillas approach is a worse fit to the longitudinal profile template (c.f. § 2.3) under the assumption that most secondaries in the shower have $E_e > 10^2$ GeV for $s \gtrsim 0.2$. Because of the latter, the results reported in this work have all been computed using the Nerling distribution.

2.3 Longitudinal Profile

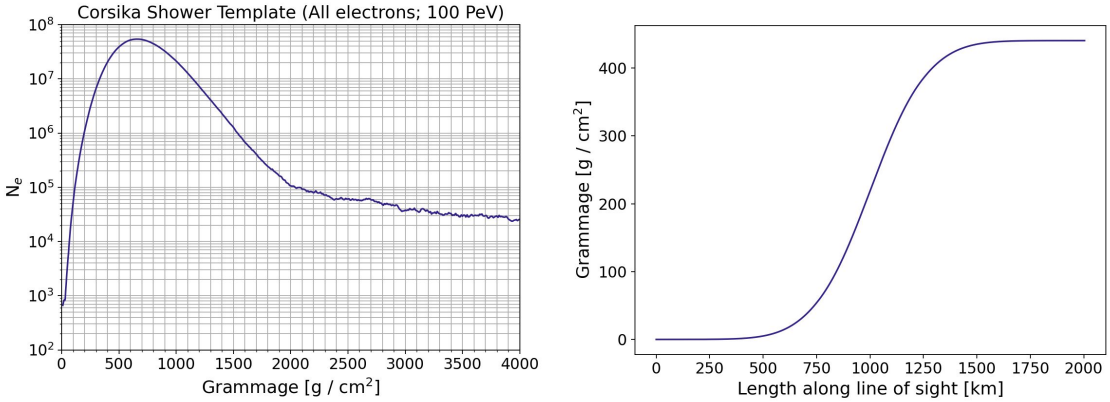

Figure 2: Longitudinal profile for a 100 PeV proton-induced shower as obtained from averaging `CORSIKA` simulations (left). An example of the grammage-length relation for a trajectory with 89 ° of viewing angle and a detector placed at z = 36 km (right). (See text for details).

In order to evaluate the shower longitudinal profile term in Eq. 2 efficiently, we use a template profile generated with the `CORSIKA` simulation framework [15], following the approach of [16, 17]. The template (shown in Fig. 2) was obtained by averaging a total of 1000 simulated proton-induced showers at 100 PeV. For different primary energies, the template was rescaled linearly in total electron size and shifted logarithmically in the position of shower maximum. We note in passing that our simulation framework admits the use of other templates for more accurate modelling of different primary energies and/or species.

Grammage values along the shower axis are assigned using the conventions of [16, 17]. Namely, the shower is developed along the line of sight from the point of atmospheric entry to a detector placed at a fixed altitude, such that the CR trajectory is fully determined by the detector height and the nadir (viewing) angle. Grammages along this axis are computed with respect to the first interaction point using US standard atmosphere density model [18]. With these conventions, each point along the shower axis is associated with its altitude, z, its distance to the first interaction point, L, the distance to the detector, $L_{\rm Det}$, and the grammage to the first interaction point, X.

2.4 Atmospheric Effects

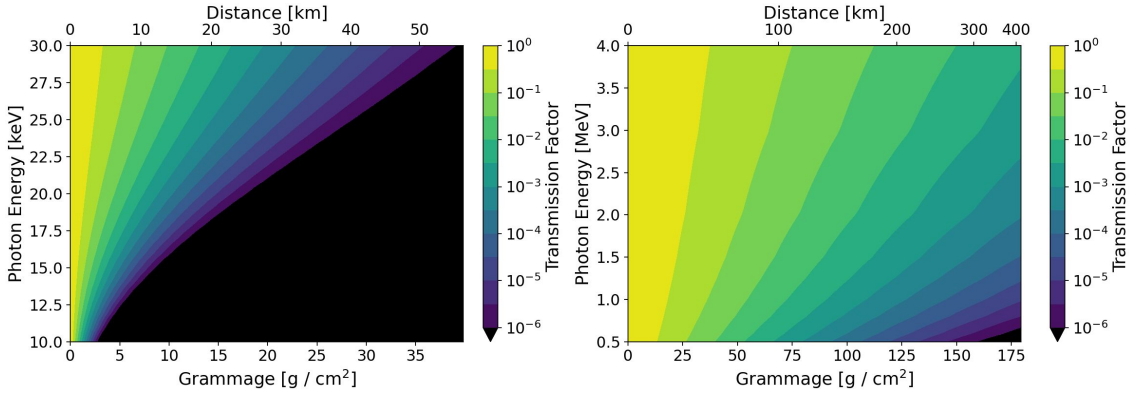

Figure 3: Contour plot of the transmission factors from the point of emission to the position of a detector at $z = 36$ km, computed according to Eq. 3, for photons in the 10 keV to 30 keV energy band (left) and for photons in the 0.5 MeV to 4.0 MeV energy band (right).

In general, the number of photons reaching the detector will not coincide with the number of photons emitted during shower development, since photons are subject to absorption and scattering in the atmosphere through several processes such as photoelectric absorption, Compton scattering, and pair production. The extent of attenuation is quantified by the mass attenuation coefficient, μ_a, which is itself derived from the photon cross section for the different absorption/scattering mechanisms. With these coefficients, the transmission factor between the emission point and the detector (or, alternatively, the survival probability) is calculated as,

$$\mathrm{Tr}\,(E_\gamma, \Delta X) = \exp\left[-\int_{L_{\rm Det}-L}^{L_{\rm Det}} \mu_{\rm a}(E_\gamma)\,\rho(z(l))dl\right] = \exp\left[-\mu_{\rm a}(E_\gamma)\Delta X\right] \tag{3}$$

where z, L, and $L_{\rm Det}$ all follow from the definitions in § 2.3, and ΔX is the grammage difference between the point of emission and the detector position.

To evaluate the transmission factors in Eq. 3, we obtained the mass attenuation factors from the NIST XCOM database [19] for a gas mixture with the same composition as the US standard atmosphere [18], assuming ideal gas behavior such that the volume and mole fractions of its constituents coincide. For the purposes of illustration, transmission factors were computed for a reference CR trajectory with 90 ° viewing angle and a detector altitude of 36 km, and are shown plotted in a colormap as a function of both the photon energy and ΔX in Fig. 3, which shows that even at sub-orbital altitudes, X-rays with energies $\sim$ 10 keV are strongly absorbed in the atmosphere, whereas gamma-rays may travel for $\gtrsim$ 100 km before being absorbed.

2.5 Illuminated Areas

The photon footprint area on the detection plane depends critically on the treatment of the electron angular and lateral distribution functions (ADF and LDF, respectively), and on the average deflections of shower electrons away from the axis due to the geomagnetic field. These ingredients are not yet well constrained in the literature for high-energy electrons at young shower ages, nevertheless we attempt here to provide a conservative estimate given the current state of the art.

For the ADF, we adopt the Bergman [20] parameterization, which has been shown to describe well the angular distribution of high-energy electrons (E $\sim$ 1 GeV to 10^3 GeV) in `CORSIKA`-simulated hadronic showers. Although this model has not been explicitly validated for young shower ages, we note that ADF parameterizations are typically a function of the electron energy only, making this choice reasonable. As for the LDF, to the best of our knowledge, no validated parameterization exists for our application. The Lafebre distributions [14], which are bivariate in shower age and electron energy, nevertheless provide evidence that lateral deviations scale as a power law in energy above $E_e > 100$ MeV, strongly suggesting that a naïve estimate based on the Molière radius in a rarefied atmosphere ($O(10\,\text{km})$) would vastly overestimate the true scale. We therefore make no attempt to extrapolate the Lafebre's results beyond their validated domain and instead use Hillas' lateral deviation formula [11], where the lateral spread is expressed as a function of the electron angular variable, which we compute from the RMS angle given by the Bergman ADF.

For each point along the shower development we compute the angular RMS and corresponding expected lateral deviation (both adjusted for magnetic deflections) and project the photon directions to the detection plane, treating the photon directions as nearly co-linear with the electron directions due to relativistic beaming. This procedure yields a grid of footprint areas as a function of electron energy and shower age. To estimate the average extent of the footprint on a given photon energy band, we perform a two-step weighted average: first over electron energy, using the Nerling distribution renormalized to the energy range relevant for that photon band, and then over shower age, with weights given by the number of transmitted photons as a function of shower age.

3. Results & Discussion

With the discussion of previous chapters in mind, the total number of photons transmitted to the detection plane is obtained by integrating the photon emission spectra (Eq. 2) corrected by the transmission factor (Eq. 3) over the full shower development, as follows,

$$\frac{dN_\gamma}{dE_\gamma} = \int_{X_{\min}}^{X_{\max}} dX \; \text{Tr}\,(E_\gamma, X_{\text{Det}} - X) \int_{E_{\min}}^{E_{\max}} \frac{dN_\gamma}{dX dE_\gamma} \tag{4}$$

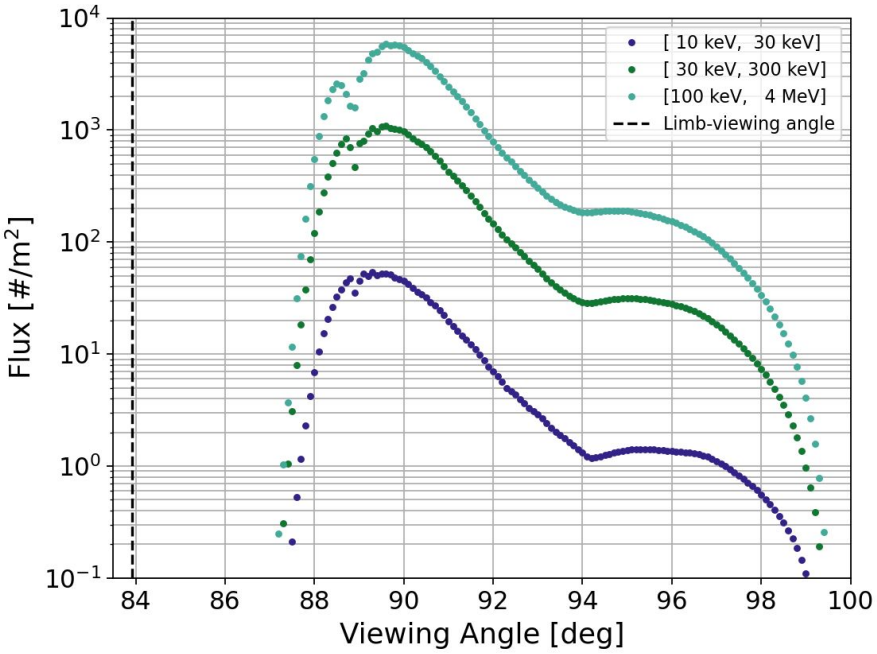

Figure 4: X-ray synchrotron fluxes for CR-induced showers at the position of a sub-orbital detector at 36 km of altitude for three different photon energy bands.

where the integration limits in electron energy are taken from 100 GeV to 1 PeV, encompassing all electrons that contribute to the synchrotron emission in the 10 keV to 10 MeV photon energy band, considering that electrons above 1 PeV are too rare to contribute significantly to the emission, even in UHE CR-induced showers. The integration limits in grammage, instead, extend from the first interaction point (fixed at 30 gcm^{-2}) up to the position of the detector (c.f. § 2.3).

The integration of Eq. 4 is done numerically on a three-dimensional grid. In particular, photon energies are sampled logarithmically from 10 keV to 10 MeV with 25 bins per decade, electron energies from 100 GeV to 1 PeV with 100 bins per decade, and grammage is sampled linearly at 10 bins per unit grammage from the first interaction point to the detector. Three photon energy bands are defined, and the number of photons transmitted to the detector in these bands is computed by integrating Eq. 4 again over the photon energy. The flux is estimated by dividing the number of transmitted photons by the estimated footprint area (for a given photon energy band) with the methods described in § 2.5. A scan over viewing angles (in 0.1 ° increments) is performed, and the results are shown in Fig. 4.

It was found that for a sub-orbital detector at $z = 36$ km, the peak of the observed flux occurs for horizontal showers with viewing angles in the range from 89 ° to 90 °. In this range, $\sim O(10^4)$ photons arrive to the detector spread out on an area $\sim O(100)$ m^2 down to $O(10)$ m^2, depending on the photon energy band. Further, it was verified that the effect of deflection of the particles by the geomagnetic field is negligible for most geometries except for viewing angles close to 89 °, which corresponds to the case of showers with a large distance to the detector from the point of first interaction that, further, develop primarily at high-altitude in a rarefied atmosphere. The effect

of these deflections is seen in the depression of the fluxes $\sim 89^\circ$ in Fig. 4. Overall, we conclude that X-ray synchrotron emission from an EAS is a signal potentially detectable by experiments at sub-orbital altitudes. It will thus the topic of future work (and of a paper under preparation) to better constraint the footprint of the emission area on the detector and to estimate the even rate that such a detector could see.

References

[1] R. Aloisio, C. Altomare, F. Barbato, R. Battiston, M. Bertania, E. Bissaldi et al., *The Terzina instrument on board the NUSES space mission*, *PoS* **ICRC2023** (2023) 391.

[2] J. Eser, A.V. Olinto and L. Wiencke, *Overview and First Results of EUSO-SPB2*, *PoS* **ICRC2023** (2023) 397.

[3] Q. Abarr, P. Allison, J. Ammerman Yebra, J. Alvarez-Muñiz, J. Beatty, D. Besson et al., *The payload for ultrahigh energy observations (pueo): a white paper*, *Journal of Instrumentation* **16** (2021) P08035.

[4] J.B. Heibges and for the JEM-EUSO Collaboration, *Poemma-balloon with radio: Mission overview*, *Journal of Physics: Conference Series* **3053** (2025) 012012.

[5] M.J. Tueros, *Simulation of radiopulses from Atmosphere-Skimming Extensive Air Showers with ZHAireS-RASPASS*, *PoS* **ARENA2022** (2023) 056.

[6] M. Tueros, S. Cabana-Freire and J. Álvarez-Muñiz, *Radio emission from atmosphere-skimming cosmic ray showers in high-altitude balloon-borne experiments*, *JCAP* **01** (2025) 112 [2409.13141].

[7] G.B. Rybicki and A.P. Lightman, *Radiative processes in astrophysics*, John Wiley & Sons (2024).

[8] R. Aloisio and P. Blasi, *Theory of synchrotron radiation: I. Coherent emission from ensembles of particles*, *Astroparticle Physics* **18** (2002) 183.

[9] R. Aloisio and P. Blasi, *Theory of synchrotron radiation: II. Backreaction in ensembles of particles*, *Astroparticle Physics* **18** (2002) 195.

[10] P. Lipari, *Concepts of "age" and "universality" in cosmic ray showers*, *Physical Review D* **79** (2009) 063001.

[11] A. Hillas, *Angular and energy distributions of charged particles in electron-photon cascades in air*, *Journal of Physics G* **8** (1982) 1461.

[12] M. Giller, G. Wieczorek, A. Kacperczyk, H. Stojek and W. Tkaczyk, *Energy spectra of electrons in the extensive air showers of ultra-high energy*, *Journal of Physics G* **30** (2004) 97.

[13] F. Nerling, J. Blümer, R. Engel and M. Risse, *Universality of electron distributions in high-energy air showers—description of cherenkov light production*, *Astroparticle Physics* **24** (2006) 421.

[14] S. Lafebre, R. Engel, H. Falcke, J. Hörandel, T. Huege, J. Kuijpers et al., *Universality of electron–positron distributions in extensive air showers*, *Astroparticle Physics* **31** (2009) 243.

[15] D. Heck, J. Knapp, J. Capdevielle, G. Schatz, T. Thouw et al., *Corsika: A monte carlo code to simulate extensive air showers*, *Report fzka* **6019** (1998) .

[16] A. Cummings, R. Aloisio, J. Eser and J. Krizmanic, *Modeling the optical cherenkov signals by cosmic ray extensive air showers directly observed from suborbital and orbital altitudes*, *Physical Review D* **104** (2021) 063029.

[17] A. Cummings, R. Aloisio and J. Krizmanic, *Modeling of the tau and muon neutrino-induced optical cherenkov signals from upward-moving extensive air showers*, *Physical Review D* **103** (2021) 043017.

[18] U.S. Atmosphere, *US standard atmosphere*, National Oceanic and Atmospheric Administration (1976).

[19] M. Berger, J. Hubbell, S. Seltzer, J. Coursey and D. Zucker, *Xcom: Photon cross section database (version 1.2)*, 1999-01-01, 1999.

[20] D. Bergman, *An efficient technique for the reconstruction of extensive air showers using non-imaging cherenkov measurements*, *Proceedings of the 33rd ICRC (Rio de Janeiro)* **983** (2013) .